


Energy density functional for α clustering and scattering of light $A = 4m$ nucleiZakaria M. M. Mahmoud **Physics Department, Faculty of Science, King Khalid University, Saudi Arabia
and Physics Department, Faculty of Science, New Valley University, El-Kharga, El-Kharga 72511, Egypt*

(Received 10 January 2022; revised 7 March 2022; accepted 22 March 2022; published 14 April 2022)

The energy density functional (EDF) is applied to study α clustering and α scattering in light $A = 4m$ nuclei. Our goal is to study the success of the EDF in predicting the ground-state α clustering in $4m$ -conjugate nuclei. The α -cluster density is obtained by optimizing the EDF with the help of the convolution theorem. The obtained cluster density reproduced the experimental binding energy of the considered nuclei. The obtained α -cluster densities are investigated through the elastic scattering of α particles from ^{12}C , ^{16}O , ^{24}Ne , ^{24}Mg , ^{28}Si , ^{32}S , and ^{40}Ca in the framework of the optical model. The real part of the optical model potential is calculated using α -cluster single folding or the conventional double folding models based on the obtained densities. The obtained potentials are used to analyze the elastic scattering of α -particle from (1) ^{12}C , ^{16}O , ^{24}Ne , ^{24}Mg , ^{28}Si , ^{32}S , and ^{40}Ca at 104 MeV, (2) ^{12}C , ^{24}Mg , and ^{28}Si at 120 MeV, (3) ^{12}C , ^{16}O , ^{24}Mg , ^{28}Si , and ^{40}Ca at 130 MeV. The obtained results are very satisfactory and in agreement with experimental data. This success indicates the validity and applicability of the EDF in α -cluster calculation for $A = 4m$ nuclei.

DOI: [10.1103/PhysRevC.105.044609](https://doi.org/10.1103/PhysRevC.105.044609)**I. INTRODUCTION**

There are many pieces of evidence that nucleons inside the nucleus tend to form clusters near the nuclear surface [1,2] (most likely α particle). Clustering in nuclei describes the emergence of molecular-like properties in the atomic nucleus, like complex rotational and vibrational excitations and intricate structural geometries. The highly symmetric α -particle (a) is enormously stable (≈ 28 MeV binding energy), (b) has a first unbound excited state at ≈ 20 MeV (that makes this four-nucleon system difficult to perturb), and (c) has spin and isospin zero (symmetric). These properties led to an early assumption that the α -particle might form a stable subunit within the nucleus. Early models of α clustering in nuclei use the clusters' geometric arrangement with a spectrum of excited states given by the dynamical symmetries. These models are improved by including the Pauli exclusion principle via antisymmetrization of the α -particle wave functions at a small separation distance. Later, different techniques for the A -body system are developed with no prior assumption of a mean-field or preexisting clusters. From these techniques, the α clustering could be derived automatically [2–10].

The α correlation should be the strongest and could be expected to behave in many respects like a free α particle. Thus, the α cluster could be used to explain the α -nucleus scattering behavior, where the enhancement of cross sections at backward angles is suggested to be related to the presence of an α correlation in the ground state of target nuclei [11]. The scattering of α particles from light heavy-ion nuclei is of special interest because elastic-scattering cross sections ex-

hibit anomalous large-angle scattering (ALAS) [12] at $E \leq 50$ MeV, or nuclear rainbow scattering [13] at $E \geq 100$ MeV. These two phenomena help to probe the nucleus-nucleus potential not only in the surface region but also at smaller distances. The interpretation of these two phenomena could play a decisive role in establishing a unique α -nucleus optical potential [12]. Therefore, an optical potential with a special radial form is needed to describe these two phenomena, for example, the powered Woods-Saxon (WS)^{*n*}, ($n \geq 2$) [14] or Michel-type [15] phenomenological potentials. Microscopic understanding of the nucleus-nucleus interaction potential is essential to understand the complex optical potential for composite systems. In addition, it helps to understand the relevant reaction dynamics involved and develop a practical tool for predicting optical potentials of colliding systems for which the elastic-scattering measurement is absent. Folding models for α -nucleus systems yielded a good account of scattering data over a wide range of energies and targets [16–22]. This indicates the success of the folding models in predicting the radial shape of real potentials. Therefore, the α -cluster model has been employed to calculate the real OMPs for composite projectiles through either the Watanabe superposition model [23] or the cluster single-folding (C-SF) [20] and cluster double-folding (C-DF) [19] models.

Kanada-En'yo *et al.* [24] analyzed the α scattering from ^{16}O at $E_\alpha = 104, 130, 146,$ and 386 MeV incident energies using the distorted-wave Born approximation (DWBA). Their α - ^{16}O potentials were constructed by folding the Melbourne g -matrix NN interaction with ^{16}O matter and transition densities calculated using variation after spin-parity projections (VAP) combined with the generator coordinate method (GCM) of the $^{12}\text{C} + \alpha$ cluster in the antisymmetrized molecular dynamics (AMD) framework. Kanada-En'yo *et al.* [25]

*zamahmoud@kku.edu.sa

analyzed α - ^{12}C scattering using the microscopic coupled channels method. Their α - ^{12}C potentials are calculated using the Melbourne g -matrix folding model. The ^{12}C matter and transition densities were calculated using the microscopic structure models of AMD and AMD + generator coordinated method (GCM). Casal *et al.* [26] used the three- and four- α -cluster molecular algebraic model to describe the scattering of α particles from ^{12}C and ^{16}O . Their optical potentials and inelastic form factors were obtained by folding densities and transition densities obtained within this molecular model. Mahmoud *et al.* [27] analyzed the α - ^{40}Ca elastic scattering over a wide range of energies and angles in the framework of the optical model over a wide range of energies and scattering angles. A semimicroscopic α -cluster model was used to compute the real optical potential with two different α - α effective interactions. The calculated real potential was supplied with an imaginary WS squared potential. Their model was found successful in reproducing the data for energies above 40 MeV.

The EDF was used to generate the real part of the α -nucleus optical potential. This potential was computed from the difference in the total energies of the two interacting nuclei at finite and infinite separation [28,29]. The success of the EDF-derived potential depends on how well the EDF reproduces the binding energies of the nuclei. In the present work, the applicability of the EDF to derive the $m\alpha$ -cluster densities for ^{12}C , ^{16}O , ^{24}Mg , ^{28}Si , ^{32}S , and ^{40}Ca nuclei are studied. The obtained densities are used to generate the real part of α -nucleus optical potentials through the C-SF and DF models. The resulting potentials were employed to analyze elastic-scattering data at 104, 120, and 130 MeV laboratory energies for the systems, $\alpha + ^{12}\text{C}$, ^{16}O , ^{24}Mg , ^{28}Si , ^{32}S , and ^{40}Ca .

II. THEORETICAL FORMALISM

The nucleus is a many-body problem with a solution that starts from the two nucleon interaction. The exact solution of the Schrödinger equation of the many-body problem is not possible, and approximations should be introduced for its solution. Statistical theory for a quantum-mechanical system shows that nuclear energy (masses) can be expressed as a unique functional of the density (EDF). The basic idea of the EDF theory is to express the total energy of the nuclear many-nucleon system as a functional $\varepsilon[\rho(r)]$ of the local density $\rho(r)$ [30–32]. In this method, the system's total energy is obtained from volume integration of the energy density functional. The variational method could be used to find the ground-state properties of the nuclear system by a minimization of the EDF with respect to the local density $\rho(r)$ functional space.

A. Energy density functional α cluster

The EDF consists of three mean parts: (1) a homogeneous term, (b) a Coulomb energy term, and (3) an inhomogeneity corrections term. The homogeneous term fits the nuclear-matter saturation curves and has the following expression [30–32]:

$$\varepsilon_{NM}[\rho(r), \alpha] = \tau[\rho(r), \alpha] + v[\rho(r), \alpha], \quad (1)$$

where the first term is a kinetic-energy term that arises from the nucleon kinetic energy in nuclear matter and is given as

$$\tau[\rho(r), \alpha] = 0.3 \left(\frac{\hbar^2}{2M} \right) \left(\frac{3\pi^2}{2} \right)^{2/3} \times [(1 - \alpha)^{5/3} + (1 + \alpha)^{5/3}] \rho^{5/3}(r), \quad (2)$$

and $v[\rho(r), \alpha]$ is the nucleonic mean-field that comes from the BHF approximation for nuclear matter and is given as

$$v[\rho(r), \alpha] = B_1(\alpha)\rho(r) + B_2(\alpha)\rho^{4/3}(r) + B_3(\alpha)\rho^{5/3}(r). \quad (3)$$

$B_1(\alpha) = b_1(1 + a_1\alpha^2)$, $B_2(\alpha) = b_2(1 + a_2\alpha^2)$, $B_3(\alpha) = b_3(1 + a_3\alpha^2)$, $\alpha = (A - 2Z)/A$ is the neutron excess, and M is the nucleon mass. The parameters [32] of the nucleonic mean field are $a_1 = -0.2$, $a_2 = 0.316$, $a_3 = 1.646$, $b_1 = -741.28$. These parameters are obtained from fitting the calculated binding energy per nucleon (E/A) to the experimental values. A Coulomb energy density should be added to the homogeneous term for finite nuclei. This Coulomb energy term is composed of two main contributions: (1) a Hartree (direct) contribution and (2) a Fock (exchange) contribution. The functional form of this Coulomb energy is approximated, to first order in e^2 by the following simple expression:

$$\varepsilon_c[\rho_p(r)] = \frac{e^2}{2} \int \frac{\rho_p(r)(r)\rho_p(r)(\tilde{r})d\tilde{r}}{|\tilde{r} - r|} - \frac{3e^2}{4} \left(\frac{3}{\pi} \right)^{1/3} \rho_p^{5/3}(r). \quad (4)$$

The last term in the EDF is the inhomogeneity-correction term. This correction represents the variation of the nucleus density at the surface. Thus, the EDF should be modified to include a gradient term (inhomogeneous corrections). The inhomogeneity term consists of two parts: (1) an exchange part and (2) a correlation part. The second part is considered in this work. This part has the form

$$\varepsilon_{\text{cor}}(\rho(r)) = \left(\frac{\hbar^2}{8M} \right) \eta [\nabla \rho(r)]^2. \quad (5)$$

η is expressed in fm^3 and will be kept as an adjustable parameter to give the correct experimental binding energies. Then the total energy density may be written as

$$\varepsilon_{\text{tot}}[\rho(r), \alpha] = \varepsilon_{NM}[\rho(r), \alpha] + \varepsilon_c[\rho(r)\alpha] + \varepsilon_{\text{cor}}[\rho(r)]. \quad (6)$$

The variational approach is the desirable and faster numerically way to deal with the EDF. In this approach, one assumes a parametrized cluster density form and searches for a minimum of EDF within this chosen functional space.

B. Nuclear density

The matter density for $4m$ mass number (m is the number of α particles) nuclei is computed from the convolution theorem as

$$\rho_m(r) = \int \rho_c(r_c)\rho_\alpha(r - r_c)d\tilde{r}_c, \quad (7)$$

where $\rho_m(r)$ is the matter density for the given nucleus of mass number A , $\rho_c(r_c)$ is the corresponding cluster density for the given nucleus, and $\rho_\alpha(r_\alpha)$ is the matter density of the α particle. By minimizing the total binding energy (6) using the density computed from Eq. (7), the density parameters of $\rho_c(r_c)$ can be obtained:

$$E = \int \varepsilon_{\text{tot}}[\rho(r), \alpha] d\vec{r}. \quad (8)$$

The form considered for $\rho_c(r_c)$ is the two-parameter Fermi (2pF) function

$$\rho_c(r_c) = \frac{\rho_0}{1 + \exp\left(\frac{r - R_c}{a_c}\right)}, \quad (9)$$

while $\rho_\alpha(r_\alpha)$ is of the simple Gaussian form as shown in Ref. [33],

$$\rho_\alpha(r) = \rho_{0\alpha} \exp(-\alpha r^2), \quad (10)$$

where $\rho_{0\alpha} = 0.4229$ and $\alpha = 0.7024$. Thus to find the cluster density parameters one should solve the variational equation

$$\frac{\delta}{\delta \rho} \int \varepsilon_{\text{tot}}[\rho(r), \alpha] d\vec{r} - E_{\text{ex}} = 0, \quad (11)$$

where E_{ex} is the experimental binding energy of the nucleus. The conservation of particle number and mean square radii are used as constraints,

$$\int \rho(r) d\vec{r} - A_T = 0, \quad (12)$$

$$\int r^2 \rho(r) d\vec{r} - \langle r^2 \rangle_{\text{ex}} = 0, \quad (13)$$

where $\int r^2 \rho(r) d\vec{r} = \langle r^2 \rangle$ and $\langle r^2 \rangle_{\text{ex}}$ are the calculated and the experimental root mean square radius, respectively, of the nucleus with mass number A_T .

C. α -cluster folded potential

To generate the real part of the α -nucleus optical potential, the double-folding DF of the matter densities of both the α particle and target nuclei with a suitable effective NN interaction may be used. But first, a semimicroscopic approach is used to construct the real part of the optical potential. In this approach, the potential is computed using an α - α interaction folded over the derived α -cluster distribution function of the target nucleus as

$$V(r) = \int \rho_c(r_c) v_{\alpha\alpha}(R - r_c) d\vec{r}_c. \quad (14)$$

The obtained potential is denoted as C-SF when used with WS imaginary potential and denoted as C-SFRI when used as real and imaginary parts with an appropriate complex renormalization factor. The α - α system has been investigated by several theoretical studies [34–37] using microscopic α - α interactions and experimental studies [38–41] using phenomenological α - α interactions. In the present work, the α - α potential of Mahmoud *et al.* [37] is considered in our calculation. This

potential has the following simple form:

$$V_{\alpha,\alpha}(r) = \sum_{i=1}^4 V_i(E_N) \exp(-\beta_i R^2). \quad (15)$$

where

$$V_1(E_N) = \frac{0.123}{2\pi^2} \sum_{j=1}^3 a_{3j} E_N^{j-1}, \quad \beta_1 = \frac{\alpha/t^2}{\alpha + 1/t^2}, \quad (16)$$

$$V_2(E_N) = \frac{0.152}{2\pi^2} \sum_{j=1}^3 a_{3j} E_N^{j-1}, \quad \beta_2 = \frac{3\alpha/t^2}{3\alpha + 4/t^2}, \quad (17)$$

$$V_3(E_N) = \frac{1.192}{2\pi^2} \sum_{j=1}^3 a_{2j} E_N^{j-1}, \quad \beta_3 = \frac{2\alpha/t^2}{2\alpha + 3/t^2}, \quad (18)$$

$$V_4(E_N) = \frac{6.125}{2\pi^2} \sum_{j=1}^3 a_{1j} E_N^{j-1}, \quad \beta_4 = \frac{\alpha/t^2}{\alpha + 2/t^2}. \quad (19)$$

This potential provides satisfactory agreement with the experimental elastic-scattering data for α - α system at energies between 6 and 280 MeV. The range parameters for this potential are $\beta_1 = 0.335 \text{ fm}^{-2}$, $\beta_2 = 0.289 \text{ fm}^{-2}$, $\beta_3 = 0.270 \text{ fm}^{-2}$, and $\beta_4 = 0.227 \text{ fm}^{-2}$, respectively, for $t = 1.25 \text{ fm}$. This effective α - α potential is based on the Jeukenne-Lejeune-Mahaux (JLM) effective NN interaction with geometrical average of the local density approximation evaluated at the position of each interacting nucleons in target and projectile. The a_{ij} parameters are given from Ref. [42]. For comparison and further confirmation of our cluster model, the DF is also used in the present work, as shown in the next section.

D. Double-folded potential

The DF model is also used to confirm the success of EDF in predicting the cluster density of the considered nuclei. The energy- and density-dependent CDM3Y6 NN effective interaction is used in the DF model. The obtained DF potential is denoted as DFM3Y when used with WS imaginary part and denoted as DFM3YRI when used as real and imaginary parts with appropriate complex renormalization factor. The CDM3Y6 effective NN interaction, $v_{NN}(|\mathbf{s}|, \rho, E)$ [43] has the following form:

$$v_{NN}(|\mathbf{s}|, \rho, E) = g(E) F(\rho) v^{D(Ex)}(|\mathbf{s}|), \quad (20)$$

where the intrinsic energy $g(E)$ and density $F(\rho)$ -dependent factors [44,45] have the following forms:

$$g(E) = 1.0 - 0.0026 \frac{E}{N}, \quad (21)$$

$$F(\rho) = 0.2658[1 + 3.8033 \exp(-1.4099\rho) - 4.0\rho]. \quad (22)$$

The radial forms of CDM3Y6 (Paris version) [44] have the following forms:

$$v^{D(Ex)}(|\mathbf{s}|) = \sum_{i=1}^3 Y^{D(Ex)}(i) \frac{\exp(-R_i |\mathbf{s}|)}{R_i |\mathbf{s}|}. \quad (23)$$

The explicit ranges and strengths parameters of these forms are given from Ref. [44]. The direct part of the real central

folded potential is computed from

$$V^D(E, R) = \int \rho_T(r_T) \rho_P(r_P) v^D(|s|, \rho, E) d^3 r_T d^3 r_P, \quad (24)$$

The exchange part of the real central folded potential is computed from

$$V^{\text{ex}}(E, R) = \int \rho_T(R, r_T) \rho_P(R, r_P) \times v^{\text{ex}}(|s|, \rho, E) j_0(k(E, R)|s|) d^3 r_T d^3 r_P, \quad (25)$$

where $j_0(x)$ is the zero-order spherical Bessel function, $\rho_{T,P}(r)$ are the target and projectile densities, respectively, and $k(E, R)$ is the relative momentum, which has the form

$$k(E, R) = \sqrt{\frac{2\mu}{\hbar^2} [E_{\text{c.m.}} - V(E, R) - V_C(r)]}. \quad (26)$$

Here μ stands for the system reduced mass, $E_{\text{c.m.}}$ is the energy in the center-of-mass system, $V_C(R)$ is the Coulomb potential, and $V(E, R) = V^D(E, R) + V^{\text{ex}}(E, R)$ is the total DF nuclear potential. The density matrix $\rho_i(R, r)$, ($i = T, P$), is considered using the following approximation:

$$\rho_i(R, r) = \rho \left(\left| R + \frac{\mathbf{s}}{2} \right| \right) j_1 \left(k_f^i \left(\left| R + \frac{\mathbf{s}}{2} \right| \right) s \right), \quad (27)$$

$$j_1(x) = 3 \frac{\sin(x) - x \cos(x)}{x^3}. \quad (28)$$

$k_f^i(r)$ is the Fermi momentum and is approximated as

$$k_f^i(r) = \sqrt{\frac{5}{3\rho_i(r)} \left(\tau_i(r) - \frac{1}{4} \nabla^2 \rho_i(r) \right)}. \quad (29)$$

The kinetic-energy density $\tau_i(r)$ is of the Thomas-Fermi approximation form [46]:

$$\tau_i(r) = \frac{3(3\pi^2)^{2/3}}{5} [\rho_i(r)]^{5/3} + \frac{|\nabla \rho_i(r)|^2}{36\rho_i(r)} + \frac{\nabla^2 \rho_i(r)}{3}, \quad i = T, P. \quad (30)$$

In the present DF model, the matter densities of the considered nuclei are computed according to Eq. (7) with the help of Eqs. (9) and (10).

III. RESULTS AND DISCUSSION

The nuclear matter density $\rho_m(r)$ of the nucleus is related to the α -particle density and its cluster density distribution inside the nucleus, $\rho_c(r)$, by Eq. (7). The 2pF form for the cluster density $\rho_c(r)$, and a simple Gaussian form for the α -particle density $\rho_\alpha(r)$, are considered in our calculation. The shape parameters of the obtained cluster density are listed in Table I. These shape parameters satisfy the following linear relations:

$$R_c = (1.477 \pm 0.057) + (0.277 \pm 0.019)A^{1/3}, \quad (31)$$

$$a_c = (-0.515 \pm 0.120) + (0.341 \pm 0.041)A^{1/3}. \quad (32)$$

TABLE I. The cluster density optimized parameters.

Nucl.	R_c fm	a_c fm	E MeV	E_{ex} MeV	$\langle r^2 \rangle$ fm ²	$\langle r_{\text{ex}}^2 \rangle$ fm ²	η fm ³
¹² C	2.115	0.205	92.179	92.2	5.400	5.388	6.00
¹⁶ O	2.202	0.353	127.58	127.6	6.767	6.730	6.45
²⁰ Ne	2.202	0.488	160.57	160.6	8.334	8.301	6.60
²⁴ Mg	2.249	0.472	198.54	198.3	8.248	8.187	6.60
²⁸ Si	2.326	0.533	236.39	236.5	9.305	9.199	6.65
³² S	2.359	0.558	271.81	271.8	9.773	9.775	6.69
³⁶ Ar	2.390	0.593	306.69	306.7	10.41	10.35	6.73
⁴⁰ Ca	2.436	0.629	342.10	342.2	11.15	11.38	6.80

ρ_{0c} in Eq. (9) is determined from the normalization condition

$$\int \rho_c(r) r^2 dr = \frac{m}{4\pi}. \quad (33)$$

These shape parameters are plotted against $A^{1/3}$ in Fig. 1. These linear relations enable us to predict the α clustering for $4m$ nuclei above ⁴⁰Ca by extrapolation and by interpolation for ⁸Be. The obtained cluster densities are shown in Fig. 2. As shown from Table I and Figs. 1 and 2, the probability of finding the α particle outside the nucleus (at the surface) increases with increasing mass number. This reflects why the η parameter increases slightly with increasing mass number. The obtained η value fits very well with the experimental binding energies [47,48] and is in agreement with that reported in Ref. [48] for ⁴⁰Ca with a Fermi-like density distribution. The

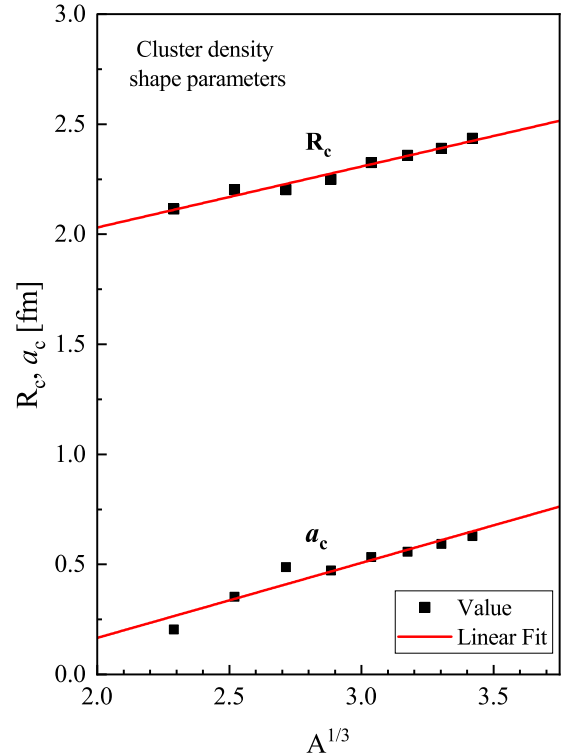


FIG. 1. Mass dependence of cluster density shape parameters.

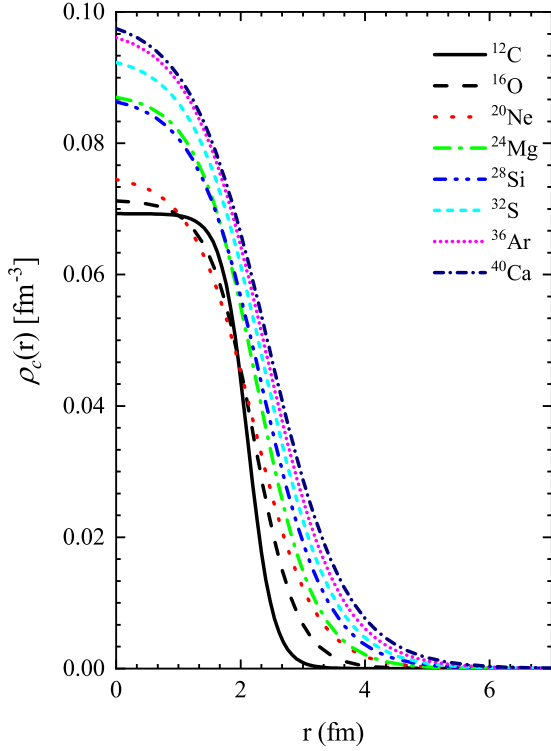


FIG. 2. α -cluster densities for ^{12}C , ^{16}O , ^{24}Ne , ^{24}Mg , ^{28}Si , ^{32}S , and ^{40}Ca nuclei.

optimized densities predict the mean square radii [49] of the considered nuclei, as shown in Table I.

To check the reliability of the obtained α -cluster densities, they are used to calculate the real α nucleus C-SF potentials for ^{12}C , ^{16}O , ^{24}Ne , ^{24}Mg , ^{28}Si , ^{32}S , and ^{40}Ca targets. The calculated potentials are used to analyze the elastic-scattering data at 104, 120, and 130 MeV α -particle incident energies. The imaginary parts of the α -nucleus optical potential are parametrized phenomenologically in a WS shape. Alternatively, the folded potential is used as an imaginary part with an appropriate imaginary renormalization factor. It is obvious that the calculated C-SF and DFM3Y potentials have depths that linearly increase with increasing target mass number and slightly decrease with increasing energy, as shown in Fig. 3. In addition, the $\langle R^2 \rangle^{1/2}$ radii is approximately energy independent for each system and linearly increase as the target mass number increases (see Fig. 4). The following relation at each energy represents this linear mass dependence:

$$Q(E) = a + bA_T. \quad (34)$$

The parameters of this relation are given in Table II.

Elastic-scattering cross-section calculations are carried out using the computer code HIOPTIM-94 [50]. The searches are carried out by optimizing four free parameters, a real renormalization factor N_R for the real calculated potentials, and the three parameters of the imaginary WS potential for C-SF and DFM3Y potentials, and the only searched parameters for C-SFRI, and DFM3YRI potentials are the real and imaginary renormalization factors N_R and N_I . The elastic-scattering data are analyzed for (1) α - ^{12}C , ^{16}O , ^{24}Ne , ^{24}Mg , ^{28}Si , ^{32}S , and

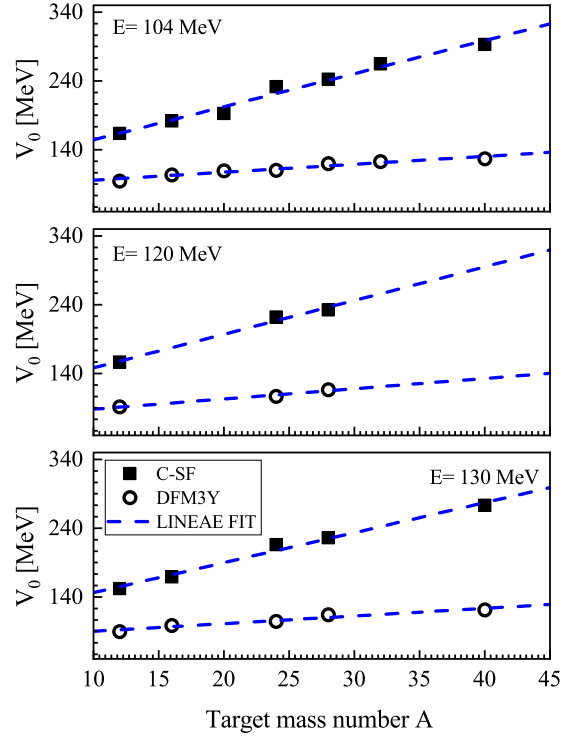


FIG. 3. Calculated potential depths target mass dependence.

^{40}Ca systems at 104 MeV, (2) α - ^{12}C , ^{24}Mg , and ^{28}Si systems at 120 MeV, and (3) α - ^{12}C , ^{16}O , ^{24}Mg , ^{28}Si , and ^{40}Ca systems at 130 MeV using the calculated potentials, respectively. The obtained best-fit optical potential parameters are listed in Tables V–VI, respectively. The calculated elastic-scattering cross sections ($d\sigma/d\sigma_R$), in comparison with experimental data [51], are shown in Figs. 5–10.

A. Cluster single-folding results

It is found that the C-SF potential yielded satisfactory reproduction of the experimental data at $E = 104, 120,$ and 130 MeV. The calculated $d\sigma/d\sigma_R$, in comparison with experimental data [51], are shown in Figs. 5–7. As shown in

TABLE II. Parameters of the linear mass dependence of potential depths V_0 and radii $\langle R^2 \rangle^{1/2}$.

$Q(E)$	E MeV	Potential	a MeV	b MeV
V_0	104	C-SF	106.09 ± 7.92	4.82 ± 0.30
		DFM3Y	84.24 ± 3.40	1.15 ± 0.13
	120	C-SF	99.15 ± 12.83	4.90 ± 0.57
		DFM3Y	73.23 ± 5.24	1.49 ± 0.23
	130	C-SF	102.64 ± 7.16	4.36 ± 0.28
		DFM3Y	79.08 ± 3.94	1.11 ± 0.15
$\langle R^2 \rangle^{1/2}$			fm	fm
	C-SF		1.741 ± 0.10	0.67 ± 0.00
	DFM3Y		1.35 ± 0.19	0.90 ± 0.07

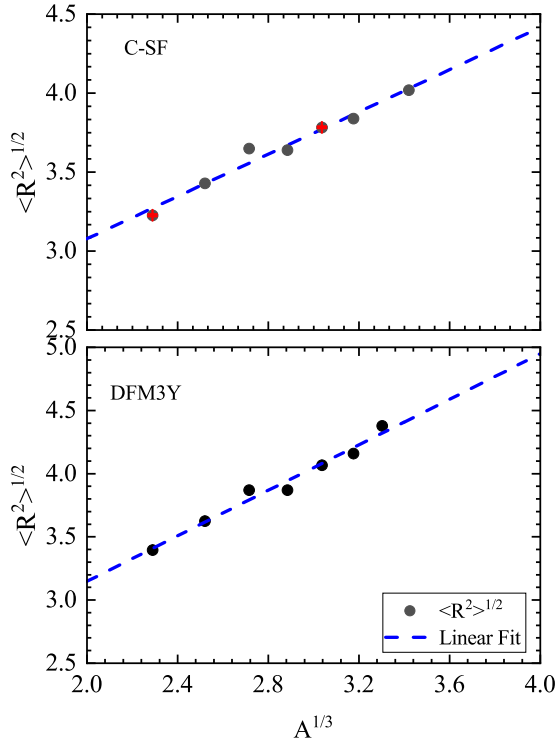


FIG. 4. Real calculated potentials $\langle R^2 \rangle^{1/2}$ for the systems α - ^{12}C , ^{16}O , ^{24}Ne , ^{24}Mg , ^{28}Si , ^{32}S , and ^{40}Ca .

Figs. 5–7, there are significant differences between the calculated cross sections using C-SF and experimental data at the mid angles in some cases. The observed pattern at these angles is due to interference between the nearside and farside scattering. Thus one expects that the present C-SF potential is not perfect in the tail region of the real part of OMP. Different potential models or effective interactions should be used to

TABLE III. Optical model fitting parameters for α -nucleus elastic scattering using C-SF OMP.

Nucl.	E MeV	N_R	W_0 MeV	r_i fm	a_i fm	J_r MeV fm ³	J_i MeV fm ³	σ_R mb
^{12}C	104	0.750	22.88	1.288	0.921	272.73	100.92	855.8
	120	0.750	16.18	1.500	0.898	261.97	95.90	839.6
	130	0.750	15.89	1.597	0.828	255.41	102.07	826.7
^{16}O	104	0.757	22.39	1.274	0.905	275.15	86.64	925.4
	130	0.756	18.30	1.429	1.001	257.45	98.75	1028
^{20}Ne	104	0.776	22.10	1.516	0.761	282.32	107.88	1076
^{24}Mg	104	0.750	49.66	1.014	1.094	272.73	130.19	1374
	120	0.750	40.58	1.117	0.997	261.97	115.57	1225
	130	0.750	43.87	1.024	1.073	255.41	114.46	1249
^{28}Si	104	0.750	61.27	0.628	1.348	272.73	102.22	1533
	120	0.750	60.22	0.848	1.065	261.97	104.79	1252
	130	0.750	62.15	0.736	1.195	255.41	102.68	1342
^{32}S	104	0.750	64.73	0.885	0.993	272.73	105.59	1281
^{40}Ca	104	0.745	84.20	0.557	1.492	270.92	119.46	2042
	130	0.760	75.59	0.724	1.235	258.82	106.69	1600

TABLE IV. The same as Table III but for DFM3Y OMP.

Nucl.	E MeV	N_R	W_0 MeV	r_i fm	a_i fm	J_r MeV fm ³	J_i MeV fm ³	σ_R mb
^{12}C	104	1.126	19.98	1.605	0.646	328.67	112.89	809.7
	120	1.122	19.45	1.579	0.729	317.43	112.29	825.0
	130	1.176	18.43	1.723	0.616	326.22	122.52	809.5
^{16}O	104	1.126	20.26	1.542	0.684	332.03	101.51	923.7
	130	1.173	16.41	1.740	0.665	328.44	111.10	965.5
^{20}Ne	104	1.072	21.02	1.627	0.821	322.50	127.06	1248
^{24}Mg	104	1.148	25.08	1.524	0.829	288.73	125.66	1300
	120	1.143	39.35	1.108	1.102	278.38	122.61	1371
	130	1.148	39.87	1.085	1.109	274.00	120.29	1342
^{28}Si	104	1.048	19.23	1.717	0.562	297.38	113.61	1239
	120	1.113	24.20	1.476	0.830	305.98	109.02	1312
	130	1.128	19.40	1.620	0.685	303.96	102.99	1231
^{32}S	104	1.066	21.14	1.703	0.407	295.54	115.50	1190
^{40}Ca	104	1.001	24.56	1.070	1.972	273.60	122.91	2842
	130	1.147	17.498	1.655	0.686	297.77	95.01	1483

see whether the cluster densities or the effective interaction are responsible for these differences.

In addition, the C-SFRI potential is used in the present analysis to reduce the number of free parameters. This folded OMP reasonably fits the experimental data over the whole angular range. The quality of fitting is not as satisfactory as that obtained using C-SF potential, especially at the energies 120 and 130 MeV. For the α - ^{12}C system as an example, the C-SF potential gives χ^2 value 8.78 (10% error) and 14.57 (experimental error) at 120 and 130 MeV, while C-SFRI gives χ^2 27.3 and 72.01 for the same energies, respectively. This means that the C-SFRI folded optical potential is not perfect

TABLE V. Optical model fitting parameters for α -nucleus elastic scattering using the C-SFRI OMP.

Nucl.	E MeV	N_R	N_I	J_R MeV fm ³	J_I MeV fm ³	σ_R mb
^{12}C	104	0.750	0.318	272.73	115.57	695.8
	120	0.750	0.328	261.97	114.50	672.8
	130	0.750	0.381	255.41	129.80	684.1
^{16}O	104	0.750	0.262	272.73	95.17	778.8
	130	0.750	0.350	255.41	119.19	787.9
^{20}Ne	104	0.750	0.364	272.73	132.43	971.4
^{24}Mg	104	0.750	0.350	272.73	127.28	1001.
	120	0.750	0.350	261.97	122.25	971.2
	130	0.750	0.350	255.41	119.19	953.2
^{28}Si	104	0.750	0.350	272.73	127.28	1095
	120	0.750	0.327	261.97	114.17	1047
	130	0.750	0.350	255.41	119.19	1045
^{32}S	104	0.750	0.355	272.73	129.16	1157
^{40}Ca	104	0.750	0.350	272.74	127.28	1289
	130	0.760	0.350	258.82	119.19	1240

TABLE VI. The same as Table V but for the DFM3YRI OMP.

Nucl.	E MeV	N_R	N_I	J_R MeV fm ³	J_I MeV fm ³	σ_R mb
¹² C	104	1.071	0.449	312.45	131.09	769.3
	120	1.056	0.455	298.76	128.60	743.2
	130	1.013	0.465	281.03	128.95	729.1
¹⁶ O	104	1.084	0.389	319.69	114.82	880.2
	130	1.102	0.463	308.60	129.67	869.5
²⁰ Ne	104	1.000	0.445	300.81	133.86	1047
²⁴ Mg	104	1.078	0.459	271.12	115.49	1050
	120	1.174	0.507	285.82	123.49	1050
	130	1.172	0.460	279.70	109.79	1010
²⁸ Si	104	1.000	0.450	283.85	127.73	1189
	120	1.075	0.466	295.56	128.03	1174
	130	1.085	0.465	292.31	125.33	1157
³² S	104	1.000	0.472	277.24	130.86	1264
⁴⁰ Ca	104	1.050	0.450	287.13	123.05	1411
	130	1.014	0.462	263.26	119.95	1366

in predicting the correct radial shape of the imaginary part, too.

The relation between the N_R and the JLM range parameter is studied for α -¹²C scattering at 104 MeV. The corresponding C-SF potential in this case is denoted as C-SFn. It is found that range parameter $t = 1.4$ could reproduce the experimental

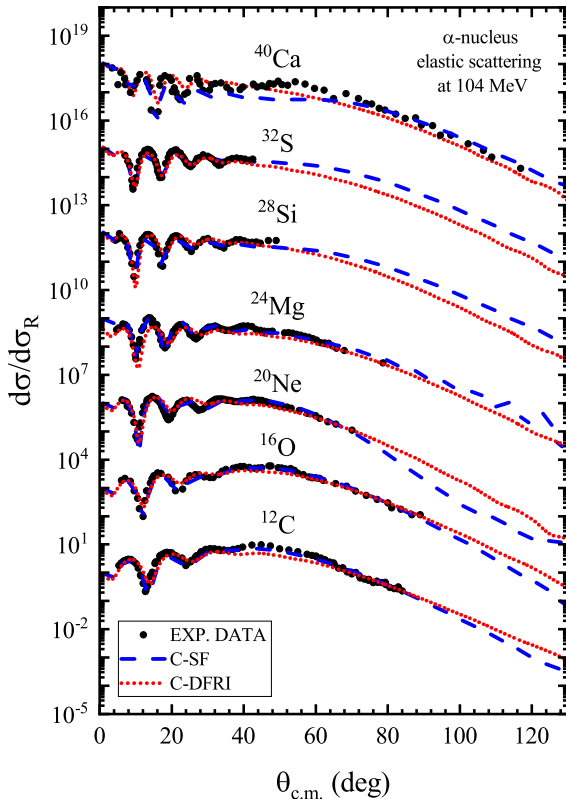


FIG. 5. Calculated $d\sigma/d\sigma_R$ for α -¹²C, ¹⁶O, ²⁴Ne, ²⁴Mg, ²⁸Si, ³²S, and ⁴⁰Ca systems at 104 MeV using C-SF and C-SFRI OMPs.

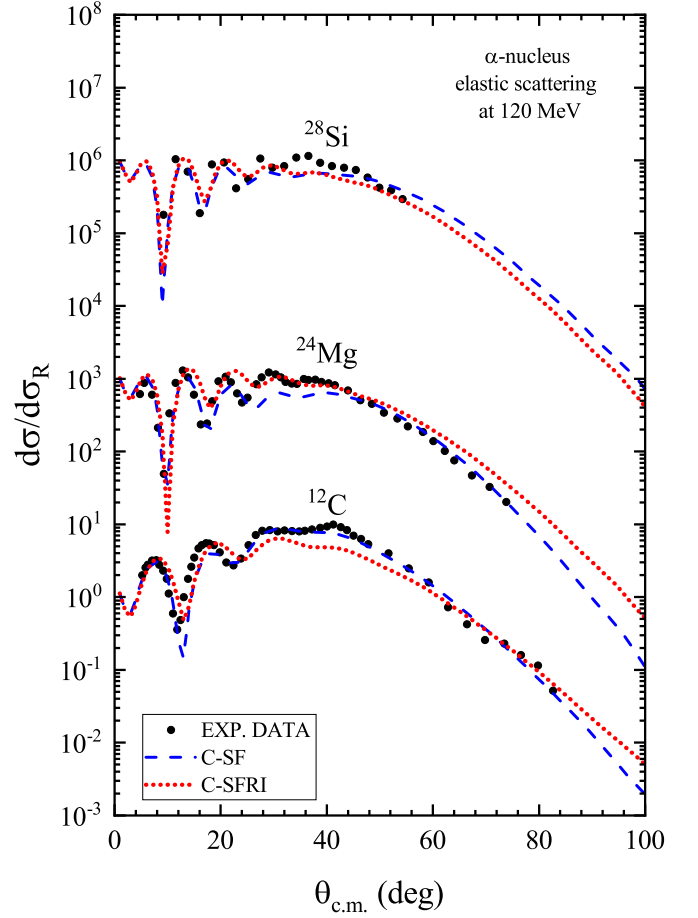


FIG. 6. Calculated $d\sigma/d\sigma_R$ for α -¹²C, α -²⁴Mg, and α -²⁸Si systems at 120 MeV using C-SF and C-SFRI OMPs.

data well with $N_R = 0.8$. This value of N_R is closed to the universal one of the JLM based potential for nucleus-nucleus scattering. That means the range parameters t and α could be slightly different from free α - α -scattering. The calculated $d\sigma/d\sigma_R$ for $t = 1.4$ are shown in Fig. 11. As shown from this figure, the C-SFn potential is as satisfactory as C-SF in reproducing $d\sigma/d\sigma_R$.

Figure 12 shows the N_R energy-dependence for C-SF, and N_R, N_I C-SFRI potentials, respectively. As shown in this figure, the C-SF potential with approximately constant $N_R \approx 0.75$ is satisfactory reproduced the experimental data for most of the considered systems. In general, the N_R for this potential has weak target mass dependence according to the following relation:

$$N_R = (0.761 \pm 0.011) - (2.439 \pm 4.303) \times 10^{-4} E. \quad (35)$$

This mass dependence is shown in the upper panel of Fig. 12.

Moreover, The C-SFRI potential with the same N_R of C-SF and slightly energy increasing N_I could be considered as satisfactory as the C-SF potential in reproducing the experimental results for all systems considered at 104 MeV and less satisfactory above this energy. In general, the many excited states involved in a nucleus-nucleus collision make the microscopic calculation of imaginary potential somewhat difficult.

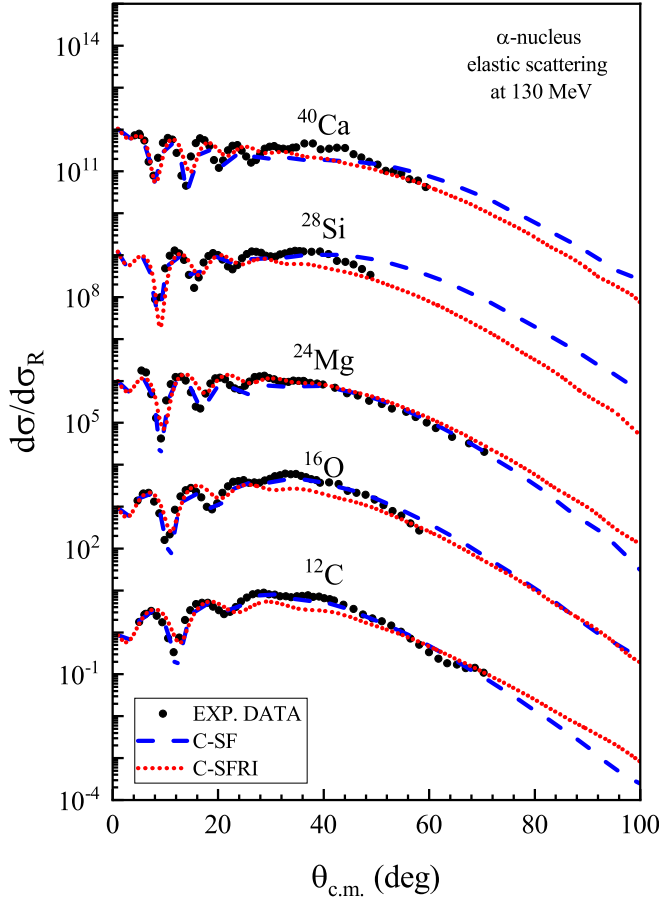


FIG. 7. Calculated $d\sigma/d\sigma_R$ for α - ^{12}C , α - ^{16}O , α - ^{24}Mg , α - ^{28}Si , and α - ^{40}Ca systems at 130 MeV using C-SF and C-SFRI OMPs.

The following relation represents N_I energy-dependence for C-SFRI potential:

$$N_I = (0.193 \pm 0.103) - (0.001 \pm 0.0)E. \quad (36)$$

B. Double-folding results

Alternatively, the DF model is used to check the reliability and the success of the present α -cluster model. For that purpose, the DFM3Y and DFM3YRI potentials are used in the present analysis. The calculated $d\sigma/d\sigma_R$ using both potentials are shown in Figs. 8–10 in comparison with the experimental data [51]. It is found that the DFM3Y potential successfully reproduces the experimental data over the whole angular range for all the considered systems. This potential is chosen because CDM3Y6 effective NN is widely and successfully used in nuclear scattering calculations and is a good test for different density models. Since the main interest is the derived densities and the success of the EDF in deriving them, the DFM3Y is used as the best choice for judging the present model. Thus the success of the DFM3Y potential indicates the applicability of EDF in predicting the α -cluster and matter densities of the considered nuclei. As shown in these figures, the difference between the calculated cross sections using DFM3Y and DFM3YRI is obvious at larger angles where experimental data do not exist for all the considered systems.

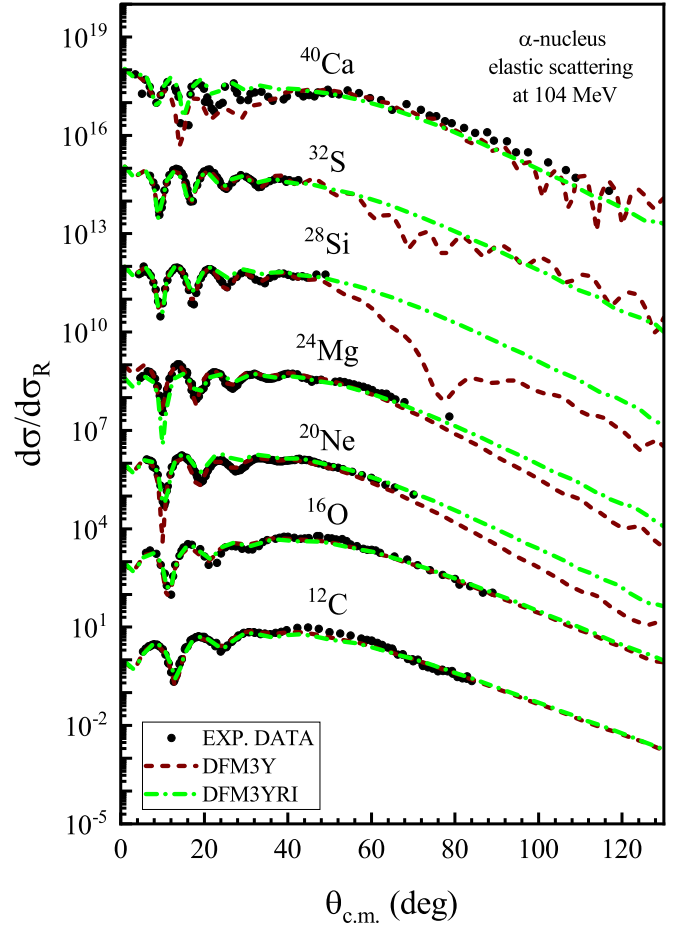


FIG. 8. Calculated $d\sigma/d\sigma_R$ for α - ^{12}C , α - ^{16}O , α - ^{24}Ne , α - ^{24}Mg , α - ^{28}Si , α - ^{32}S , and α - ^{40}Ca systems at 104 MeV using DFM3Y and DFM3YRI OMPs.

Also, there are differences between the calculated cross sections using both potentials at the mid-angles. In this range of angles, the DFM3YRI underestimates the calculated cross sections for some cases. That means the imaginary folded potential is not as successful as the flexible WS imaginary one. Although the DFM3YRI is still very satisfactory in reproducing the experimental data, which also confirms the success of the present α -cluster model for the considered nuclei. The best fitting N_R values for DFM3Y is approximately constant with energy with a small deviation about a mean value for each system. So, the mass dependence is studied for the N_R . This mass dependence is shown in the upper panel in Fig. 12. It is found that the N_R has a clear mass-dependence according to the following relation:

$$N_R = (1.173 \pm 0.033) - (0.003 \pm 0.001)A_T. \quad (37)$$

As shown in Fig. 12, N_R for DFM3YRI is approximately mass independent (N_R fluctuated around mass-averaged value with slight deviation). This mass-averaged value has a linear energy dependence according to the following relation:

$$N_R = (0.840 \pm 0.160) + (0.002 \pm 0.001)E. \quad (38)$$

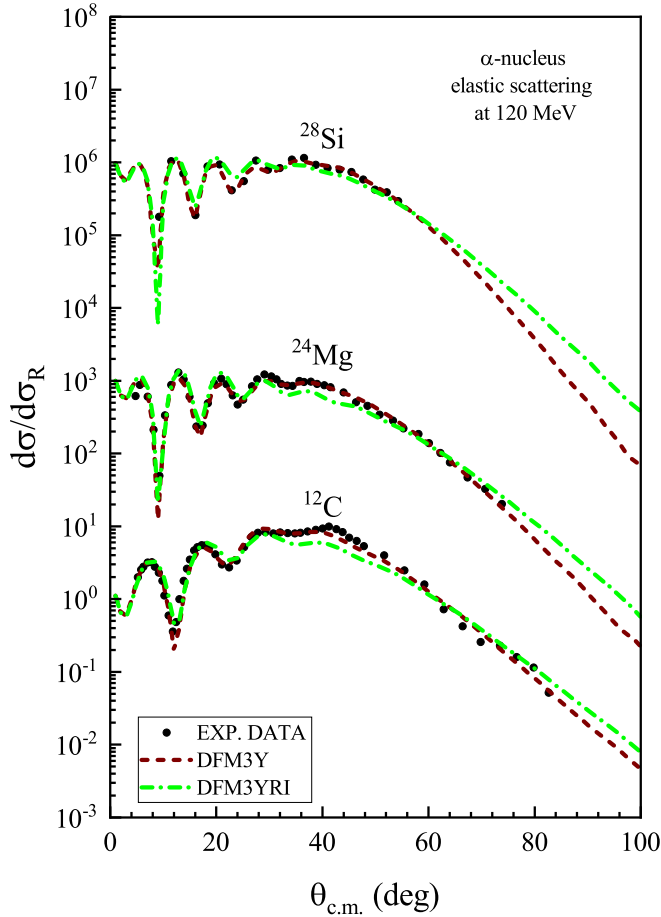


FIG. 9. Calculated $d\sigma/d\sigma_R$ for α - ^{12}C , α - ^{24}Mg , and α - ^{28}Si systems at 120 MeV using DFM3Y and DFM3YRI OMPs.

The corresponding N_I is approximately constant with average value 0.403 ± 0.084 . This energy dependence of the real and imaginary renormalization factors for both C-SFRI and DFM3YRI potentials are shown in the mid and lower panels in Fig. 12, respectively.

C. Comparison with previous studies

The present calculations, especially for DFM3Y potential, are as satisfactory as those obtained using phenomenological optical potentials [15,52–55] or those using microscopic DF potentials [22,33,56–59]. Our calculations reproduce the elastic-scattering data quite well compared with recent calculations based on the α -cluster model [24–27]. First, it is found that our model reproduces ^{12}C and ^{16}O matter radii in good agreement with that found by Kanada-En’yo *et al.* [24,25]. All our calculated potentials reproduce the elastic-scattering data much better than that found in Refs. [24,25] for α - ^{12}C at 130 MeV and for ^{16}O at 104 and 130 MeV. In Refs. [24,25], they restricted their analysis to the angular range below 40° , while our analysis extended to the whole range of the experimental data. As shown in Figs. 5–10, our results agree with that found by [24,25] up to 15° , and beyond this angle, our calculations become closer and well reproduce the experimental data, especially for C-SF and DFM3Y potentials,

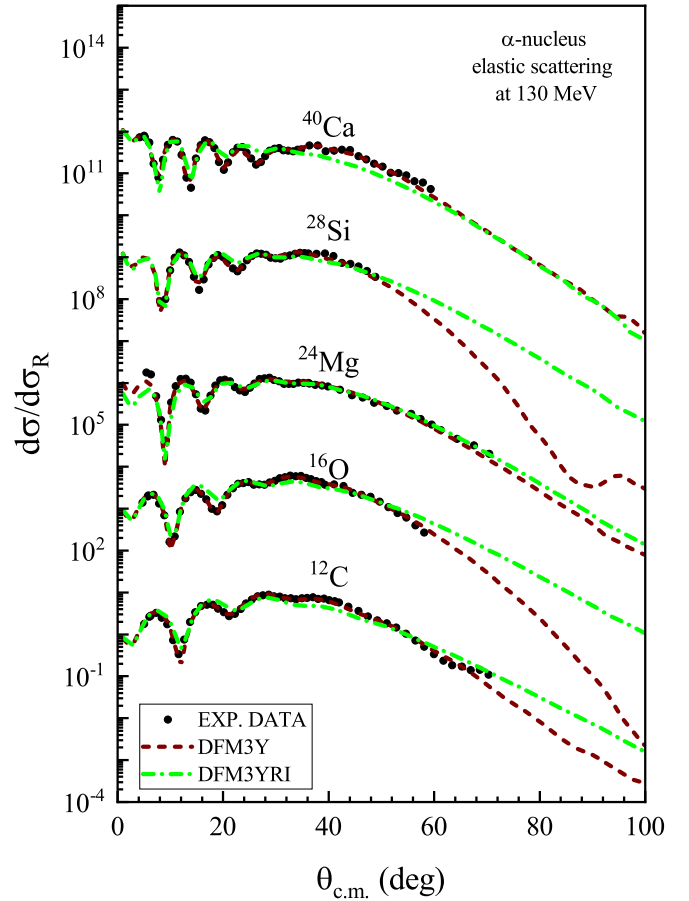


FIG. 10. Calculated $d\sigma/d\sigma_R$ for α - ^{12}C , α - ^{16}O , α - ^{24}Mg , α - ^{28}Si , and α - ^{40}Ca systems at 130 MeV using DFM3Y and DFM3YRI OMPs.

respectively. Also, our results for α - ^{16}O elastic scattering at 130 MeV is found to be better than that in Ref. [26]. In Ref. [26], the elastic-scattering calculations deviated from the data as the scattering angle increased, while our results successfully described the data over the whole angular range. For consistency, the present DFM3YRI calculation is compared with their calculations. It is found that the DFM3YRI with weak energy-dependence N_R and approximately constant $N_R \approx 0.403 \pm 0.084$ could reproduce successfully and capture the main features of the experimental data compared with their model. Kanada-En’yo *et al.* [60,61] analyzed the scattering of α particles from ^{24}Mg using the microscopic coupled-channel approach by folding the Melbourne g -matrix NN interaction with the antisymmetrized molecular dynamic densities of ^{24}Mg . Their study reasonably reproduced the elastic and inelastic cross sections angular distributions of the existing data at an energy range of $E_\alpha = 100$ – 400 MeV. They restricted their analysis to the angular range below 40° . It is found that our calculations are better in agreement with the experimental data over the whole angular range than that found by Kanada-En’yo *et al.* [60,61] at the corresponding energies. Also, our results for α - ^{40}Ca elastic scattering is in agreement with that of Mahmoud *et al.* [27] at 104 MeV. The present cluster model reproduces the $d\sigma/d\sigma_R$ as successfully

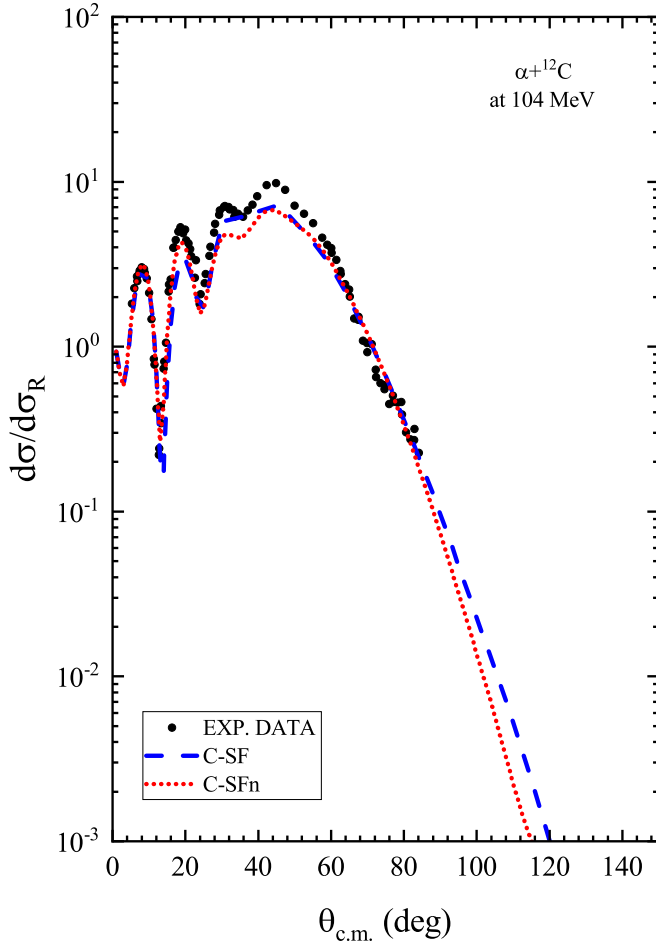


FIG. 11. Calculated $d\sigma/d\sigma_R$ for α - ^{12}C at 104 MeV using C-SFn with $t = 1.4$ (dotted line) in comparison with C-SF (long dashed line) and experimental data (solid circles).

as that obtained by Wei *et al.* [62]. This comparison with these microscopic cluster models confirms that the present α -cluster model could successfully predict the $d\sigma/d\sigma_R$ over the whole angular range, especially when using DFM3Y and DFM3YRI potentials.

In addition, the present results are compared with that based on the conventional DF calculations [21,62–64]. Our results agree with that found by Wei *et al.* [62] for α - ^{12}C , ^{16}O , ^{28}Si , and ^{40}Ca elastic scattering at the corresponding energies. References [21,62] used microscopic nucleus-nucleus OMP obtained by double folding the complex JLM effective interaction with the matter densities of both projectile and target nuclei. Their calculated cross sections were in good agreement with the experimental data, which confirms the applicability of our cluster model. Also, our present DFM3Y potential reproduced the elastic scattering of α - ^{12}C , ^{16}O as successful as that obtained by Khoa *et al.* One can see from the figures that the DFM3Y potential is the best choice for the real optical model potential [63]. Khoa *et al.* [63] tested various density models for the α -particle and target nucleus. They found that α -nucleus potential is quite sensitive to the density models. Thus, the folding potential's success depends

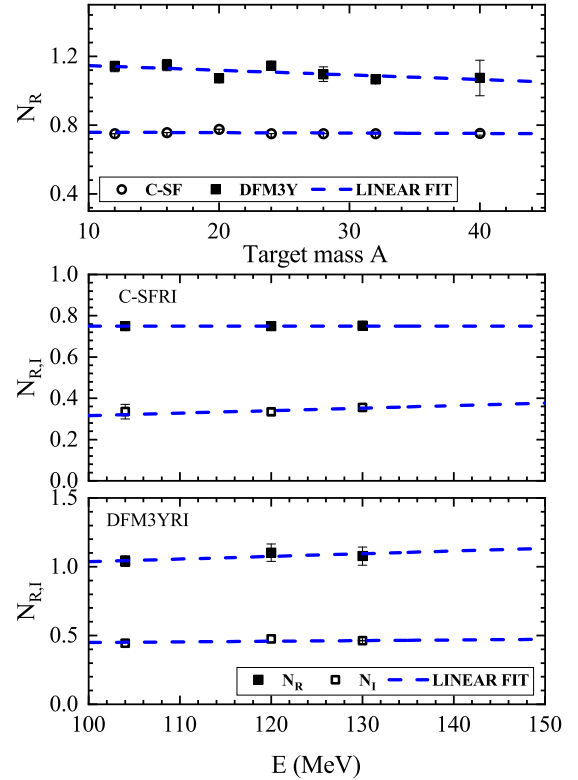


FIG. 12. N_R , target mass-dependence for C-SF and DFM3Y (upper panel), and the energy dependence of N_R , N_I for C-SFRI (middle panel), and DFM3YRI (lower panel).

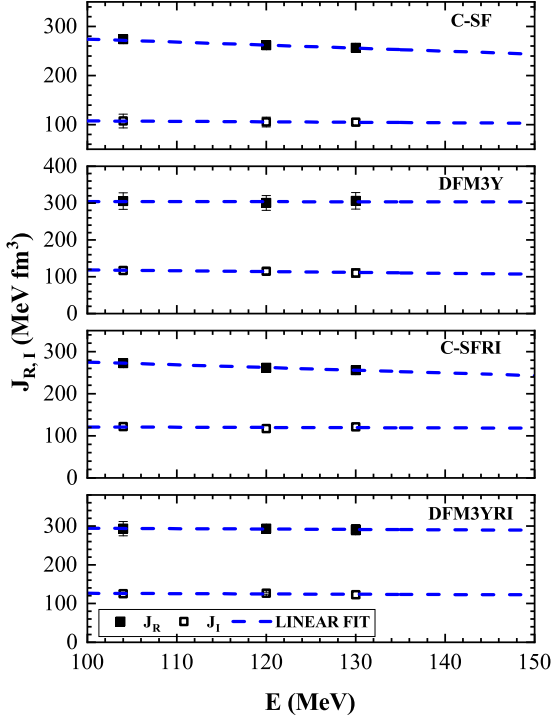
on choosing the correct density distribution. This indicates that the present derived density successfully describes the ground state α -clustering in the considered nuclei. That means the success of our present EDF α -cluster model.

D. Volume integrals

Usually, the strengths of nuclear optical potentials can be compared in terms of either the well depths or the volume integrals per projectile-target nucleon pair. Since the geometries of the potentials could be different, the volume integrals per projectile-target nucleon pair is the standard way to compare different potentials. As shown in Fig. 13, all the calculated potentials have approximately mass-independence real and imaginary volume integrals J_R and J_I , respectively. These J_R and J_I decrease linearly with increasing energy according to the following relation:

$$J_k(E) = a + bE, \quad k = R, I. \quad (39)$$

The parameters of this relation is presented in Table VII. All our calculated potentials belong to the same potential family with volume integral around 350 MeV fm^3 . As shown in Fig. 13 and Table VII, the J_R for both C-SF and C-SFRI potentials have approximately the same energy dependence. Our results for C-SF and C-SFRI potentials are lower in value for each system than that found in Ref. [21] except for α - ^{40}Ca . For α - ^{12}C , our J_R values are in agreement with that found in Refs. [20,33,62]. In addition, these two potentials have J_R

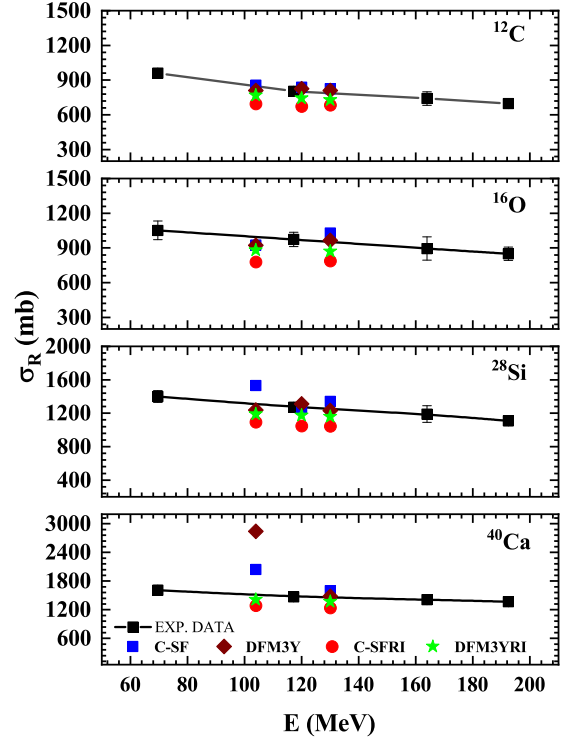
FIG. 13. Energy dependence of the volume integrals J_R and J_I .

values in good agreement with those obtained by Michel *et al.* [15] from their global phenomenological optical potential analysis of α - ^{16}O elastic scattering. The J_I has a saturation value $\approx 110 \text{ MeV fm}^3$. This result coincides exactly with that found by Refs. [20,21,33,62] using the microscopic potentials based on the cluster-folded potential and agree with the results of the references reported therein, for $E \geq 100 \text{ MeV}$. The new renormalized C-SFn potential has larger $\langle R_R^2 \rangle^{1/2}$ (3.31 fm) and J_R (328.83 MeV fm^3) than the old one and is closed to that of the renormalized DFM3Y potential ($\langle R_R^2 \rangle^{1/2} = 3.39$, $J_R = 328.67 \text{ MeV fm}^3$) and other previous studies [63].

For DFM3Y potential, it found that both J_R and J_I are approximately mass independent, and slightly decreased with increasing energy. This energy dependence also follows the linear relation given by Eq. (39). Both DFM3Y and DFM3YRI potentials have approximately the same en-

TABLE VII. Parameters of the linear energy dependence of J_R and J_I .

J(E)	Potential	a MeV fm ³	b MeV fm ³
J_R	C-SF	335.533 ± 11.963	-0.613 ± 0.099
	DFM3Y	305.330 ± 29.066	-0.013 ± 0.245
	C-SFRI	339.473 ± 2.699	-0.643 ± 0.023
	DFM3YRI	303.610 ± 9.839	-0.096 ± 0.083
J_I	C-SF	117.003 ± 3.073	-0.094 ± 0.023
	DFM3Y	140.917 ± 9.990	-0.225 ± 0.085
	C-SFRI	126.500 ± 23.849	-0.054 ± 0.201
	DFM3YRI	134.349 ± 15.48	-0.080 ± 0.131

FIG. 14. Energy dependence of the total reaction cross section σ_R .

ergy dependence and slightly decrease with increasing energy compared with the C-SF and C-SFRI ones. The results for DFM3Y potential are in agreement with that found in Refs. [15,20,21,33]. The corresponding average imaginary volume integral has a saturation value $\approx 112 \text{ MeV fm}^3$. This result is also in good agreement with that found by Refs. [20,21,33,62] using the microscopic potentials based on the cluster folded potential. This comparison for volume integrals with previous studies add another confirmation about the success of our present cluster model.

E. Total reaction cross sections

Studying total reaction cross section σ_R is an active field of study in nuclear physics. σ_R represents the probability that the projectile nucleus undergoes a nonelastic process. Reaction cross-section data are essential to verify the analysis of elastic-scattering reactions and to find a unique optical potential. It can be used to eliminate any optical potential ambiguities or compare between different potential models. In the present work, the calculated total reaction cross sections are compared with that produced by previous analyses and the available measured values [65]. As shown in Fig. 14, the obtained reduced reaction cross sections using C-SF and DFM3Y potentials are in agreement with that predicted by other microscopic [33,63] and are close to that obtained experimentally [65] for α - ^{12}C , α - ^{16}O , and α - ^{28}Si . That means our deep real folding model potential could predict σ_R in better agreement with experiments data. This comparison adds another confirmation about the success of the present α -cluster model.

IV. SUMMARY AND CONCLUSION

In this work, the EDF is employed to study α clustering for ^{12}C , ^{16}O , ^{24}Ne , ^{24}Mg , ^{28}Si , ^{32}S , ^{36}Ar , and ^{40}Ca . The EDF is optimized to reproduce the binding energy of the considered nuclei through a variational procedure. The obtained densities fit the experimental binding energy and precisely predict the root mean square radii for the considered nuclei. The shape parameters of the obtained cluster densities show clear target-mass dependence. This mass dependence enables one to predict the cluster density for nuclei not considered in this study by interpolation or extrapolation.

To check the reliability of present α -cluster model, the obtained densities are implemented to calculate α -nucleus potential for the targets ^{12}C , ^{16}O , ^{24}Ne , ^{24}Mg , ^{28}Si , ^{32}S , and ^{40}Ca , using α - α or CDM3Y6 effective interactions. The calculated potentials reproduced $d\sigma/d\sigma_R$ as satisfactory as those obtained in previous phenomenological and microscopic optical potential analyses for the all the systems considered. The C-SF, DFM3Y potentials N_R values are approximately energy independent but slightly decrease as the target mass number increases. For C-SFRI and DFM3YRI potentials, the N_R and N_I values are found approximately mass independent but with weak energy dependence. It is obvious from this analysis that the DFM3Y is the best potential choice for the description of experimental data. Also, it is expected that the C-SF model potential could represent the experimental data well if a proper effective α - α is used. The real volume integrals have decreasing energy-dependent behavior with increasing energy for all the calculated potentials. However, the imaginary volume integrals for all the calculated potential have a saturation value in this rainbow scattering region. These real and imaginary volume integrals are in agreement with that found in previous studies for most of the considered systems, which support the present α -cluster model.

As another confirmation of the success of the present α -cluster model, the calculated total reaction cross sections are compared with those obtained in previous analyses using phenomenological, microscopic potentials, and direct measurements. It is found that our calculated ones are in good agreement with those reported in those studies. This agreement add confirmation about the success of the present α -cluster model.

In conclusion, it is found that the EDF could be used successfully in predicting and calculating the ground state α -cluster density of $4m$ nuclei, ($m \leq 9$). This success is mostly supported by the success of DFM3Y potential in describing the experimental elastic-scattering data. Also, it is expected that the α particle inside the nuclei should be slightly different from the free one, and this may be one reason for the value of $N_R \approx 0.75$ for C-SF and C-SFRI potentials. This value indicates that the α -particle radius parameter or the effective potential range parameter t could differ from the values used. To investigate that the correlation between N_R and t -parameter in α - α effective interaction is studied for α - ^{12}C elastic scattering at 104 MeV. It is found that there is a correlation between this parameter and the renormalization factor.

For future work, the range parameter of the α -particle density will be subject to variation in the EDF optimization procedure, or a different α -density form should be used to simulate the medium effects on the α particle.

ACKNOWLEDGMENT

The author extends his appreciation to the Deanship of Scientific Research at King Khalid University for funding this work through research groups program under Grant No. R.G.P.2/104/41.

-
- [1] P. E. Hodgson, Alpha clustering in nuclei, *Contemp. Phys.* **31**, 99 (1990).
 - [2] M. Freer and A. C. Merchant, Developments in the study of nuclear clustering in light even-even nuclei, *J. Phys. G* **23**, 261 (1997).
 - [3] R. Bijker and F. Iachello, The algebraic cluster model: Three-body clusters, *Ann. Phys. (NY)* **298**, 334 (2002).
 - [4] V. Della Rocca, R. Bijker, and F. Iachello, Single-particle levels in cluster potentials, *Nucl. Phys. A* **966**, 158 (2017).
 - [5] M. Freer, H. Horiuchi, Y. Kanada-En'yo, D. Lee, and Ulf-G. Meißner, Microscopic clustering in light nuclei, *Rev. Mod. Phys.* **90**, 035004 (2018).
 - [6] Y. Kanada-En'yo, M. Kimura, and A. Ono, Antisymmetrized molecular dynamics and its applications to cluster phenomena, *Prog. Theor. Exp. Phys.* **2012**, 01A202 (2012).
 - [7] Y. Kanada-En'yo, Variation after Angular Momentum Projection for the Study of Excited States Based on Antisymmetrized Molecular Dynamics, *Phys. Rev. Lett.* **81**, 5291 (1998).
 - [8] Y. Kanada-En'yo, H. Horiuchi, and A. Ono, Structure of Li and Be isotopes studied with antisymmetrized molecular dynamics, *Phys. Rev. C* **52**, 628 (1995).
 - [9] Y. Kanada-En'yo, Deformations in $n = 14$ isotones, *Phys. Rev. C* **71**, 014303 (2005).
 - [10] Y. Kanada-En'yo and H. Horiuchi, Clustering in yrast states of ^{20}Ne studied with antisymmetrized molecular dynamics, *Prog. Theor. Phys.* **93**, 115 (1995).
 - [11] F. Michel, α -clustering in the ground state of ^{40}Ca , *Phys. Lett. B* **60**, 229 (1976).
 - [12] Th. Delbar, Gh. Grégoire, G. Paic, R. Ceuleneer, F. Michel, R. Vanderpoorten, A. Budzanowski, H. Dabrowski, L. Freindl, K. Grotowski, S. Micek, R. Planeta, A. Strzalkowski, and K. A. Eberhard, Elastic and inelastic scattering of alpha particles from $^{40,44}\text{Ca}$ over a broad range of energies and angles, *Phys. Rev. C* **18**, 1237 (1978).
 - [13] D. T. Khoa, Exchange effects in nuclear rainbow scattering, *Nucl. Phys. A* **484**, 376 (1988).
 - [14] H. P. Gubler, U. Kiebele, H. O. Meyer, G. R. Plattner, and I. Sick, The phenomenological optical potential for α -scattering from nuclei in the Ca region, *Nucl. Phys. A* **351**, 29 (1981).
 - [15] F. Michel, J. Albinski, P. Belery, Th. Delbar, Gh. Grégoire, B. Tasiaux, and G. Reidemeister, Optical model description of $\alpha + ^{16}\text{O}$ elastic scattering and alpha-cluster structure in ^{20}Ne , *Phys. Rev. C* **28**, 1904 (1983).

- [16] H. Abele, H. J. Hauser, A. Körber, W. Leitner, R. Neu, H. Plappert, T. Rohwer, G. Staudt, M. Straßer, S. Weite, M. Walz, P. D. Eversheim, and F. Hinterberger, Measurement and folding-potential analysis of the elastic α -scattering on light nuclei, *Z. Phys. A: Atom. Nucl.* **326**, 373 (1987).
- [17] H. Abele and G. Staudt, α - ^{16}O and α - ^{15}N optical potentials in the range between 0 and 150 MeV, *Phys. Rev. C* **47**, 742 (1993).
- [18] D. T. Khoa, G. R. Satchler, and W. von Oertzen, Nuclear incompressibility and density dependent NN interactions in the folding model for nucleus-nucleus potentials, *Phys. Rev. C* **56**, 954 (1997).
- [19] M. E. Farid, Z. M. M. Mahmoud, and G. S. Hassan, Analysis of heavy ions elastic scattering using the double folding cluster model, *Nucl. Phys. A* **691**, 671 (2001).
- [20] M. E. Farid, Z. M. M. Mahmoud, and G. S. Hassan, α -clustering folding model, *Phys. Rev. C* **64**, 014310 (2001).
- [21] T. Furumoto and Y. Sakuragi, Application of the Jeukenne-Lejeune-Mahaux folding model to α -nucleus elastic scattering, *Phys. Rev. C* **74**, 034606 (2006).
- [22] K. O. Behairy, Z. M. M. Mahmoud, and M. Anwar, Alpha-particle elastic scattering from ^{12}C , ^{16}O , ^{24}Mg , and ^{28}Si , *Nucl. Phys. A* **957**, 332 (2017).
- [23] S. A. E. Khallaf, A. L. El-Attar, and M. E. Farid, Elastic scattering of ^{12}C ions using the Watanabe superposition model, *J. Phys. G: Nucl. Phys.* **8**, 1721 (1982).
- [24] Y. Kanada-En'yo and K. Ogata, First microscopic coupled-channels calculation of cross sections for inelastic α scattering off ^{16}O , *Phys. Rev. C* **99**, 064608 (2019).
- [25] Y. Kanada-En'yo and K. Ogata, α scattering cross sections on ^{12}C with a microscopic coupled-channels calculation, *Phys. Rev. C* **99**, 064601 (2019).
- [26] J. Casal, L. Fortunato, E. G. Lanza, and A. Vitturi, Alpha-induced inelastic scattering and alpha-transfer reactions in ^{12}C and ^{16}O within the algebraic cluster model, *Eur. Phys. J. A* **57**, 33 (2021).
- [27] Z. M. M. Mahmoud and K. O. Behairy, α -cluster optical potential model of ^{40}Ca , *Braz. J. Phys.* **47**, 189 (2017).
- [28] P. Manngård, M. Brenner, M. M. Alam, I. Reichstein, and F. B. Malik, Molecular potential and elastic scattering of alpha particles by ^{28}Si from 14 to 28 MeV, *Nucl. Phys. A* **504**, 130 (1989).
- [29] M. M. Billah, M. N. A. Abdullah, S. K. Das, M. A. Uddin, A. K. Basak, I. Reichstein, H. M. Sen Gupta, and F. B. Malik, Alpha-Ni optical model potentials, *Nucl. Phys. A* **762**, 50 (2005).
- [30] K. A. Brueckner, J. R. Buchler, R. C. Clark, and R. J. Lombard, Statistical Theory of Nuclei. II. Medium and Heavy Nuclei, *Phys. Rev.* **181**, 1543 (1969).
- [31] K. A. Brueckner, J. R. Buchler, S. Jorna, and R. J. Lombard, Statistical theory of nuclei, *Phys. Rev.* **171**, 1188 (1968).
- [32] S. Hossain, M. N. A. Abdullah, Md Rahman, A. K. Basak, and F. Malik, Non-monotonic potentials for ^6Li elastic scattering at 88 MeV, *Phys. Scr.* **87**, 015201 (2013).
- [33] Z. M. M. Mahmoud, K. O. Behairy, A. A. Ibraheem, S. R. Mokhtar, M. A. Hassanain, and M. E. Farid, Analysis of alpha scattering from α -conjugate nuclei, *J. Phys. Soc. Jpn.* **88**, 024201 (2019).
- [34] G. R. Satchler and W. G. Love, Folding model potentials from realistic interactions for heavy-ion scattering, *Phys. Rep.* **55**, 183 (1979).
- [35] Z. M. M. Mahmoud, A. A. Ibraheem, and M. E. Farid, Alpha-alpha potentials in a wide range of energies, *J. Phys. Soc. Jpn.* **81**, 124201 (2012).
- [36] M. E. Farid, Microscopic description of $^4\text{He} + ^4\text{He}$ elastic scattering over the energy range $e = 100\text{--}280$ MeV, *Phys. Rev. C* **74**, 064616 (2006).
- [37] Z. M. M. Mahmoud and M. A. Hassanien, Analytical $\alpha + \alpha$ potential for energy range between 6 and 280 MeV, *Phys. At. Nucl.* **83**, 418 (2020).
- [38] V. G. Neudatchin, V. I. Kukulin, V. L. Korotkikh, and V. P. Korennoy, A microscopically substantiated local optical potential for α - α scattering, *Phys. Lett. B* **34**, 581 (1971).
- [39] B. Buck, H. Friedrich, and C. Wheatley, Local potential models for the scattering of complex nuclei, *Nucl. Phys. A* **275**, 246 (1977).
- [40] L. Marquez, Alpha-alpha potential, *Phys. Rev. C* **28**, 2525 (1983).
- [41] P. Darriulat, G. Igo, H. G. Pugh, and H. D. Holmgren, Elastic scattering of alpha particles by helium between 53 and 120 MeV, *Phys. Rev.* **137**, B315 (1965).
- [42] J.-P. Jeukenne, A. Lejeune, and C. Mahaux, Optical-model potential in finite nuclei from Reid's hard core interaction, *Phys. Rev. C* **16**, 80 (1977).
- [43] D. T. Khoa, G. R. Satchler, and W. von Oertzen, Folding analysis of the elastic $^6\text{Li} + ^{12}\text{C}$ scattering: Knock-on exchange effects, energy dependence, and dynamical polarization potential, *Phys. Rev. C* **51**, 2069 (1995).
- [44] D. T. Khoa, E. Khan, G. Colò, and N. Van Giai, Folding model analysis of elastic and inelastic proton scattering on sulfur isotopes, *Nucl. Phys. A* **706**, 61 (2002).
- [45] Do Cong Cuong, D. T. Khoa, and Y. Kanada-En'yo, Folding-model analysis of inelastic $\alpha + ^{12}\text{C}$ scattering at medium energies, and the isoscalar transition strengths of the cluster states of ^{12}C , *Phys. Rev. C* **88**, 064317 (2013).
- [46] M. Y. H. Farag, E. H. Esmael, and H. M. Maridi, Analysis of proton- $^9,^{10,11,12}\text{Be}$ scattering using an energy-, density-, and isospin-dependent microscopic optical potential, *Phys. Rev. C* **90**, 034615 (2014).
- [47] J. H. E. Mattauch, W. Thiele, and A. H. Wapstra, 1964 atomic mass table, *Nucl. Phys.* **67**, 1 (1965).
- [48] M. A. Hooshyar, I. Reichstein, and F. B. Malik, *Nuclear Fission and Cluster Radioactivity* (Springer, Berlin, Heidelberg, 2005).
- [49] H. De Vries, C. W. De Jager, and C. De Vries, Nuclear charge-density-distribution parameters from elastic electron scattering, *At. Data Nucl. Data Tables* **36**, 495 (1987).
- [50] N. M. Clarke, Hi-optim 94.2 code, University of Birmingham (private communication, 1994).
- [51] Nuclear Data Base, 1999–2005, <https://www-nds.iaea.org/>.
- [52] S. M. Smith, G. Tibell, A. A. Cowley, D. A. Goldberg, H. G. Pugh, W. Reichart, and N. S. Wall, *Nucl. Phys. A* **207**, 273 (1973).
- [53] G. Hauser, R. Löhken, H. Rebel, G. Schatz, G. W. Schweimer, and J. Specht, Elastic scattering of 104 MeV alpha particles, *Nucl. Phys. A* **128**, 81 (1969).
- [54] D. A. Goldberg, Improved six-parameter alpha-nucleus optical potentials, *Phys. Lett. B* **55**, 59 (1975).
- [55] F. R. Lichtenhaler, A. C. C. Villari, A. Lepine-Szily, and L. C. Gomes, Inversion potential for the $\alpha + ^{12}\text{C}$ system, *Phys. Rev. C* **44**, 1152 (1991).

- [56] S. A. E. Khallaf, A. M. A. Amry, and S. R. Mokhtar, Elastic scattering analysis of α and ${}^3\text{He}$ particles on ${}^{12}\text{C}$ and ${}^{16}\text{O}$ using a complex folded potential, *Phys. Rev. C* **56**, 2093 (1997).
- [57] A. H. Amer, Yu. E. Penionzhkevich, and A. Amar, Optical and double folding model analysis of ${}^{28}\text{Si}(\alpha, \alpha){}^{28}\text{Si}$ elastic scattering from 12.7 to 240 MeV, *Phys. Part. Nucl. Lett.* **18**, 640 (2021).
- [58] A. H. Amer, Yu. E. Penionzhkevich, A. A. Ibraheem, and Sh. Hamada, Comparison between the elastic scattering of ${}^{12}\text{C}(\alpha, \alpha){}^{12}\text{C}$ and ${}^{12}\text{C}({}^6\text{He}, {}^6\text{He}){}^{12}\text{C}$ using different nuclear potentials, *Int. J. Mod. Phys. E* **29**, 2050086 (2020).
- [59] D. T. Khoa, W. von Oertzen, H. G. Bohlen, and S. Ohkubo, Nuclear rainbow scattering and nucleus-nucleus potential, *J. Phys. G* **34**, R111 (2007).
- [60] Y. Kanada-En'yo and K. Ogata, Probing negative-parity states of ${}^{24}\text{Mg}$ probed with proton and α inelastic scattering, *Phys. Rev. C* **103**, 024603 (2021).
- [61] Y. Kanada-En'yo and K. Ogata, Microscopic coupled-channel calculation of proton and alpha inelastic scattering to the 4_1^+ and 4_2^+ states of ${}^{24}\text{Mg}$, *Prog. Theor. Exp. Phys.* **2021**, 043D01 (2021).
- [62] W. Zou, Y. Tian, and Z.-Y. Ma, Microscopic optical potential for α -nucleus elastic scattering in a Dirac-Brueckner-Hartree-Fock approach, *Phys. Rev. C* **78**, 064613 (2008).
- [63] D. T. Khoa, α -nucleus optical potential in the double-folding model, *Phys. Rev. C* **63**, 034007 (2001).
- [64] A. H. Amer, Z. M. M. Mahmoud, and Yu. E. Penionzhkevich, Double folding analysis of $\alpha + {}^{12}\text{C}$ elastic scattering using different effective interactions, *Nucl. Phys. A* **1020**, 122398 (2022).
- [65] A. Ingemarsson, J. Nyberg, P. U. Renberg, O. Sundberg, R. F. Carlson, A. J. Cox, A. Auce, R. Johansson, G. Tibell, D. T. Khoa, and R. E. Warner, New results for reaction cross sections of intermediate energy α particles on targets from ${}^9\text{Be}$ to ${}^{208}\text{Pb}$, *Nucl. Phys. A* **676**, 3 (2000).